PCCP

ROYAL SOCIETY OF CHEMISTRY

PAPER

View Article Online
View Journal

Cite this: DOI: 10.1039/d6cp00202a

First water-to-ligand substitution dictates Co^{2+}/Ni^{2+} extraction selectivity

Kailong Zhang,[a] Yuxuan Zhang,[a] Bin Ji,[b] Rick Honaker,[b] Isabel C. Escobar,[c] Jian Shi[a] and Qing Shao*[c]

Solvent extraction is a crucial technology for the large-scale recovery of critical metals. One key challenge is to develop ligands with high ionic selectivity, especially for ions with similar properties. Manipulating ionic solvation emerges as a viable approach to enhance the selectivity. However, such manipulation requires a thorough understanding of the thermodynamics underlying ligand-induced variation in ionic solvation. We investigated the thermodynamics governing the binding of two organophosphorus ligands (Cyanex 272 and D2EHPA) with Co^{2+} and Ni^{2+} at the aqueous-organic liquid–liquid interface using a combination of experiments and computations. UV-vis and IR spectroscopy confirmed that extraction induces solvation structure changes of Ni^{2+} and Co^{2+}. The free-energy landscapes obtained from well-tempered metadynamics illustrated two plausible routes for water–ligand substitution during extraction. In the first route, the ligand occupies the vacancy created by the departing water molecule. In the second route, the ligand associates with the ion to form an oversaturated solvation state that drives water expulsion. The ligand-binding process is a competition between the two routes. The free-energy landscapes further revealed that substitution of the first water molecule in the ionic solvation shell plays a determining role in ligand-induced ionic selectivity. Our results suggest a target for the rational design of Co^{2+}/Ni^{2+} separation technology: engineering the free energy associated with substitution of the first water molecule.

Received 20th January 2026,
Accepted 1st June 2026

DOI: 10.1039/d6cp00202a

rsc.li/pccp

Introduction

Cobalt and nickel are critical metals essential for many modern technologies, including rechargeable batteries, catalysts, and magnetic devices.[1,2] Recovering cobalt and nickel from spent devices, such as multi-metallic cathodes of used batteries, has become an important secondary supply route. A key aspect of the recycling process is achieving selective separation of Ni^{2+} and Co^{2+} in the post-leaching solutions. However, cobalt and nickel are adjacent in the periodic table, and their cations exhibit nearly identical ionic radii and coordination chemistry. Achieving high selectivity remains a challenge.[3,4]

Solvent extraction is a scalable technology for cobalt and nickel separation, but its development is hindered by a limited mechanistic understanding of ionic selectivity.[5,6] In solvent extraction, metal ions are selectively transferred from the aqueous solution into an immiscible organic phase containing extractant ligands. Organophosphorus acids, such as Cyanex 272 (bis(2,4,4-trimethylpentyl)phosphinic acid, BTP) and D2EHPA (bis(2-ethylhexyl) phosphate, BEP), are the most common choices in current solvent extraction processes.[3,7] At the molecular level, the extraction occurs through ion transfer and complexation at the aqueous-organic interface. The metal ions and extractant headgroups first migrate to the interface, where the ions subsequently coordinate with the donor atoms of the extractant headgroups to form metal–ligand complexes.[8,9] The extractant's hydrophobic tails then solubilize the complexes and carry them into the organic phase.[10,11] Recent studies have focused on interfacial phenomena in solvent extraction. For example, several studies have examined how extractant solubility influences interfacial complexation and extraction efficiency.[10,11] However, one ultimate goal of such chemical separation is to achieve high selectivity. The current knowledge remains limited to guide the design and optimization of this target.

Water–ligand substitution at the liquid–liquid interface plays a decisive role in extraction selectivity.[5] The aqueous-organic interfacial region provides a heterogeneous chemical environment, where the dielectric discontinuity, disrupted hydrogen-bond network, and amphiphilic organization of extractant molecules modulate and reconstruct ion solvation.[9,12] At the interface, water molecules and extractant ligands compete to occupy the first solvation shell of the ions. The solvation structure reorganizes as water molecules are stepwise replaced by

[a] Department of Biosystems and Agricultural Engineering, University of Kentucky, Lexington, KY 40506, USA
[b] Department of Mining Engineering, University of Kentucky, Lexington, KY, 40506, USA
[c] Department of Chemical and Materials Engineering, University of Kentucky, Lexington, KY 40506, USA. E-mail: qshao@uky.edu

extractant headgroups.[13–15] Manipulating ionic solvation has proven to be a powerful strategy for tuning the selectivity of ions with similar properties.[16,17] However, the complexity of the interface, including its nanoscopic heterogeneity and transient, metastable coordination intermediates, makes direct characterization of solvation changes challenging.[18] Yet, a comprehensive theoretical framework to guide the ionic solvation manipulation in solvent extraction is still incomplete.

Two fundamental questions remain about the water–ligand substitution. First, does one or several specific water–ligand substitution steps dominate the extraction free energy? One cation is coordinated by multiple water molecules. The water–ligand substitution during extraction involves multiple steps to replace the water molecules in the ionic solvation shell with ligand molecules. The individual substitution steps are expected to yield different free energy changes because they occur in a changing environment. These differences and their roles in extraction thermodynamics remain unclear. Second, what route may each water–ligand substitution step follow? We hypothesize two possible routes for a single water–ligand substitution step. The first is a vacate-and-fill route: a coordinated water molecule dissociates, leaving a vacant site that the ligand then fills. The second is an oversaturate-and-release route: a ligand enters the solvation shell to form an overcoordinated complex, which subsequently expels a water molecule. Do the two routes have similar free energy barriers and contribute equally to substitution, or does one route thermodynamically dominate the substitution process?

To answer these questions, we investigate water–ligand substitution during the solvent extraction of Co^{2+} and Ni^{2+} using two ligands (BTP and BEP). We first use spectroscopic measurements and molecular dynamics (MD) simulations to characterize changes in ionic solvation structure upon extraction. We then employ well-tempered metadynamics (WT-MetaD) to analyse the thermodynamics of water–ligand substitution at the aqueous–organic liquid–liquid interface. WT-MetaD introduces a history-dependent bias along chosen collective variables (CVs) to enhance sampling of the free-energy landscape.[19,20] This approach has been successfully applied in related contexts, such as mapping the lanthanide solvation landscape and determining the free-energy pathways of zeolitic imidazolate framework self-assembly.[21,22] Here, we use WT-MetaD to determine the free-energy landscapes of water–ligand substitution in the solvation shell of Co^{2+} and Ni^{2+} at the liquid–liquid interface. Other factors, such as electronic-structure effects, are outside the focus of the present WT-MetaD study. We modelled the aqueous–organic interface where metal extraction occurs (Fig. S1). We show that the first water–ligand substitution step possesses the highest energy cost and dictates the selectivity. Co^{2+}/Ni^{2+} extraction selectivity can be tuned through ligand-dependent $\Delta\Delta F$ at this initial substitution step. Our simulations quantify how the known Co^{2+}/Ni^{2+} periodic trend affects the free-energy barrier of the water-to-ligand substitution within the ionic solvation shell. This work provides the molecular foundation for understanding extraction free energies and guides the rational design of ion-selective solvent extraction systems by identifying the dominant free-energy contributors and the key mechanistic step governing extraction.

Results and discussion

Change in Co^{2+} and Ni^{2+} solvation upon extraction

Shifts in the UV-vis spectra indicate distinct changes in Co^{2+} and Ni^{2+} solvation upon extraction. We measured the UV-vis spectra for Co^{2+} and Ni^{2+} in three media: the initial aqueous solution and the organic phases obtained after extraction with BTP or BEP (Fig. 1). For each initial aqueous solution, three metal ion concentrations (0.025, 0.05, and 0.10 M) were prepared and subjected to solvent extraction. Co^{2+} in the aqueous solution exhibits a broad absorption band around 512 nm, corresponding to d–d electronic transitions in the octahedral $[Co(H_2O)_6]^{2+}$ complex.[23] Upon extraction into the organic phase, the colour changed visually from pink in the aqueous solution to dark blue in the organic phase, and its absorption spectrum exhibited a red shift and resolved into multiple distinct peaks. For the Co^{2+} extracted with BTP, three absorption maxima at 548 nm, 588 nm, and 634 nm were observed. The spectra of Co^{2+} extracted with BEP are similar to those with BTP; however, the absorption peaks are blue shifted by ~6 nm. For Ni^{2+}, the UV-vis spectrum in aqueous solution exhibits a prominent absorption band at ~394 nm and a broad and weak band near 720 nm. Upon extraction into the organic phase, no visible colour change is observed. However, the primary absorption band exhibits a slight red shift, appearing at ~406 nm in the BTP system and ~401 nm in the BEP system. These spectral shifts indicate changes in the solvation of Co^{2+} and Ni^{2+} and suggest the formation of new coordination complexes with the ligands upon extraction.[23,24]

The FTIR spectra confirm ligand coordination and reveal their binding sites (Fig. 2). FTIR spectra were measured for the organic phases after extraction with BTP and BEP. BTP exhibits a characteristic absorption band corresponding to the phosphoryl (P═O) stretching vibration at 1175 cm^{-1}, along with a P–O–H stretching band at 947 cm^{-1}.[25] For BEP, the P═O stretching vibration appears at 1235 cm^{-1}, and a P–O–C stretching band is observed at 1030 cm^{-1}.[26] The P═O band for both BTP and BEP exhibits a pronounced red shift with increasing concentrations of Co^{2+} and Ni^{2+}, from 1175 to 1135 cm^{-1} for BTP and from 1235 to 1195 cm^{-1} for BEP. This

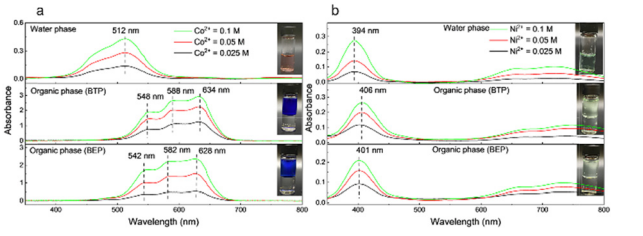

Fig. 1 UV-vis spectra of initial aqueous and organic solutions after extraction of (a) Co^{2+} and (b) Ni^{2+}. The metal ion concentrations in the initial aqueous solutions were 0.025 M, 0.05 M, and 0.1 M, and the solutions were then subjected to extraction.

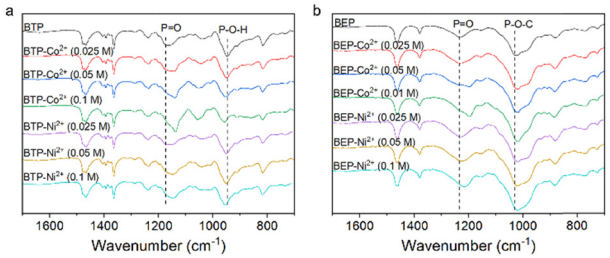

Fig. 2 FTIR spectra of organic solutions obtained after extraction of Co^{2+} and Ni^{2+} at concentrations of 0.025 M, 0.05 M, and 0.1 M with (a) BTP or (b) BEP.

red shift reflects electron density withdrawal from the P═O bonds upon complexation, indicating their role as primary donor sites. The extent of the red shift increased with higher metal ion concentrations, corresponding to increased ligand substitution. P–O–C stretching bands in BEP experienced a very weak red shift owing to the delocalized electron density of the alkoxy oxygen, as well as steric hindrance from the alkyl substituents, which makes this site less favourable for direct coordination with Co^{2+} or Ni^{2+} than P═O. These results suggest that the P═O oxygen atoms of BTP and BEP serve as primary binding sites for Co^{2+} and Ni^{2+}.

Solvation structure of Co^{2+} and Ni^{2+}

The solvation structures of Co^{2+} and Ni^{2+} in aqueous and organic solutions show six donor oxygen atoms in the first solvation shell, with the Ni–O coordination distance being slightly shorter than the Co–O distance. MD simulations were performed to characterize the solvation structures of Co^{2+} and Ni^{2+} in aqueous and organic solutions. As shown in Fig. 3, Co^{2+} and Ni^{2+} exhibit sharp first-shell peaks in the radial distribution functions (RDFs) at 0.21 and 0.20 nm, respectively, in the aqueous solution. In the BTP- and BEP-organic solutions, the two ions coordinate to the ligand oxygen atoms of the P═O donors. The coordination distances are 0.20 nm for Co–O_{BTP}, 0.20 nm for Co–O_{BEP}, 0.20 nm for Ni–O_{BTP}, and 0.19 nm for Ni–O_{BEP}. In both aqueous and organic solutions, the cumulative coordination numbers (CNs) reach ~6, indicating approximately 6 oxygen atoms in water or the extractant ligand for a saturated coordination sphere (Fig. 3). Previous studies using X-ray absorption spectroscopy and MD simulations have also reported a similar solvation structure for Co^{2+} in aqueous solution, with six water molecules

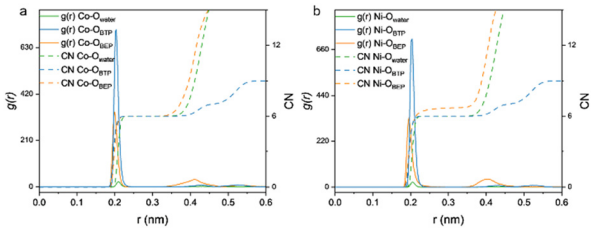

Fig. 3 Radial distribution functions (RDFs) and corresponding coordination numbers (CNs) of (a) Co^{2+} and (b) Ni^{2+} with respect to oxygen atoms in water, BTP, and BEP.

in the first solvation shell at Co–O distances of ~0.21 nm.[27] Ni^{2+} was reported to adopt an octahedral first solvation shell with six water molecules at Ni–O distances of ~0.20 nm.[28] For organic-phase solvation, a previous study reported a similar coordination structure for Co^{2+} and Ni^{2+}, with each metal ion bound by six monodentate $[Tf_2N]^-$ ligands.[29] Due to the slightly smaller ionic radius, Ni^{2+} forms shorter and stronger Ni–O bonds, resulting in a more rigid solvation shell and consequently more difficult water substitution compared to Co^{2+}.[30] We note that secondary RDF peaks are also observed for the metal ions with respect to water, BTP, and BEP. However, these peaks are significantly weaker and reflect longer-range, indirect interactions.[8] Therefore, in this work, we focus our analysis on the first solvation shell.

Free energy landscapes

We performed WT-MetaD to determine the free-energy landscapes of water–ligand substitution at the liquid–liquid interface based on the ion-O(ligand) CN (CV1), and the ion-O(water) CN (CV2). The simulation details are provided in the supplementary information (SI). The sampling range for the two CVs was set to 0–6.5 based on the RDF analysis. For each system, the CV space was sampled using three overlapping subwindows and stitched into a global landscape. The WT-MetaD trajectories extend to 1000–2000 ns, depending on the subwindow systems. The convergence analysis showed closely overlapping one-dimensional free-energy profiles and errors mostly below 5 kJ mol^{-1}. We also recorded the location of the cation during the WT-MetaD simulations. The interfacial region was defined from the *z*-dependent density profiles of water, *n*-heptane, and extractant molecules. We assigned the interface to the region where the aqueous and organic density profiles overlap and vary most strongly. For the BTP-Co^{2+} system, this region is approximately 3.3–4.3 nm, as shown in Fig. S5. The unbiased metal-ion z-position sampled during WT-MetaD remains mainly within this region, indicating that the water-to-ligand substitution events analysed here occur at the liquid–liquid interface.

The free-energy landscape shows the water–ligand substitution as a multi-stage process. Fig. 4 presents the free-energy landscape of the BTP-Co^{2+} system. The lowest free-energy basin is located near CN (Co–O_{BTP}) = 6 and CN (Co–O_{water}) = 0, corresponding to a fully extractant-substituted solvation shell. We define this state as the thermodynamic reference minimum with Helmholtz free energy F = 0 kJ mol^{-1}. Local free-energy basins appear at integer coordination numbers, with the lower-energy states distributed along the diagonal (total CN = 6). These basins correspond to relatively stable solvation configurations with varying degrees of water–ligand substitution. Snapshots in Fig. 4 show the corresponding solvation structures of these intermediates. The energy landscape shows an anti-correlation between Co–O_{BTP} and Co–O_{water} coordination: as the CN of BTP extractant increases, the CN of water correspondingly decreases. Highly water-coordinated states with few or no bound BTP ligands lie at higher free energies (>150 kJ mol^{-1}), whereas extractant-rich coordination states are more stable (lower free energy). This steep energetic penalty drives the replacement of water molecules by BTP ligands and promotes formation of the

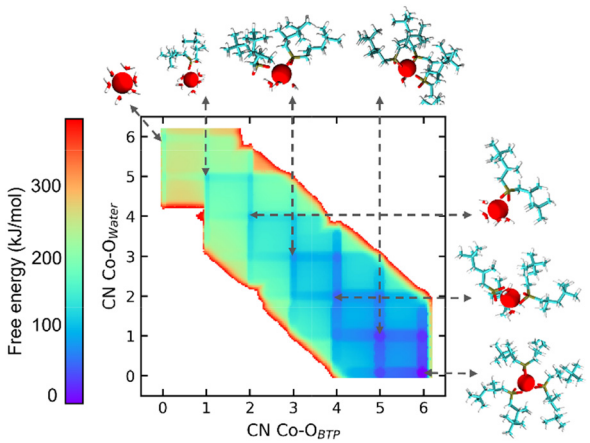

Fig. 4 Free-energy landscape of Co^{2+} as a function of the coordination number (CN) of Co–O_{BTP} and Co–O_{Water}. Representative snapshots of solvation intermediates at local minima show coordination transitions during ligand substitution. Snapshots are extracted from the WT-MetaD trajectory of the BTP-Co^{2+} system. Red sphere: Co^{2+}. Ligand atom colours: C, cyan; O, red; P, tan; H, white.

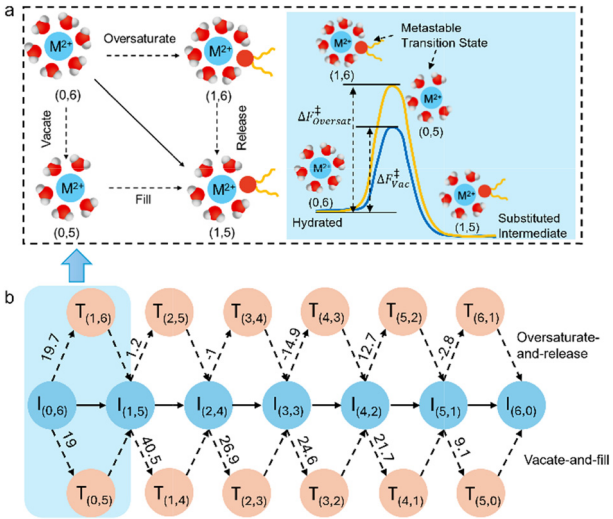

Fig. 5 Ligand substitution proceeds with vacate-and-fill and oversaturate-and-release routes in the BTP-Co^{2+} system. (a) Illustration of single-step ligand substitution in which one ligand oxygen replaces a coordinated water molecule. (b) Free-energy barriers (in kJ mol^{-1}) of solvation-shell substitution *via* vacate-and-fill or oversaturate-and-release routes. Each solvation state is represented as (CN_O–ligand, CN_O–water).

metal ion-extractant complex. Such a thermodynamic preference is directly related to the ion transfer from the aqueous phase (more water coordinated) into the organic phase (more extractant substituted).[9]

Two routes for water–ligand substitution

The free-energy landscape identifies the two water–ligand substitution routes proposed above: vacate-and-fill and oversaturate-and-release. As shown in Fig. 5a, the vacate-and-fill route begins with the loss of a coordinated water molecule to create a vacant coordination site (CN = 5), which is subsequently occupied by the extractant ligand. In contrast, in the oversaturate-and-release route, the extractant ligand binds first, increasing the coordination number to an oversaturated state (CN = 7), after which a water molecule departs. From each solvation intermediate (total CN = 6), both substitution routes are viable to reach the next coordination state. The relative likelihood of these two routes is inferred from their free-energy barriers on the WT-MetaD landscape. Thus, they describe probabilistic transitions between adjacent six-coordinate solvation states (Fig. 5a). We examined the energetics of the two routes at each intermediate coordination state (0,6), (1,5), (2,4), (3,3), (4,2), and (5,1). The free-energy barriers are shown in Fig. 5b and Table S1. At the beginning of substitution, *i.e.*, the transition from the fully water-coordinated state (0,6) to the singly substituted state (1,5), the vacate-and-fill route exhibits slightly smaller free-energy barriers across all four systems, indicating that it is more favourable. During the second oxygen substitution, *e.g.*, from (1,5) to (2,4), the reaction proceeds through the oversaturate-and-release route. This is because once the first donor oxygen has coordinated to the metal ion, the ligand is already in the first solvation shell, and its second donor oxygen is more accessible. Therefore, the vacate-and-fill and oversaturate-and-release routes represent two general limiting pathways for solvation-shell solvent–ligand substitution. The preferred route and energy barrier depend on factors such as the extractant structure, hydration strength, and interfacial environment.

Ligand-substitution pathway shows similar patterns across the four systems, with vacate-and-fill route dominating the first step and oversaturate-and-release routes dominating the remaining steps. By evaluating the free-energy profiles of the vacate-and-fill and oversaturate-and-release routes at each intermediate state, we identified the most thermodynamically favourable ligand-substitution pathway. The pathways for all four systems are summarized in Fig. 6. The coordination states along these pathways are labelled as a–m. All four systems exhibit similar

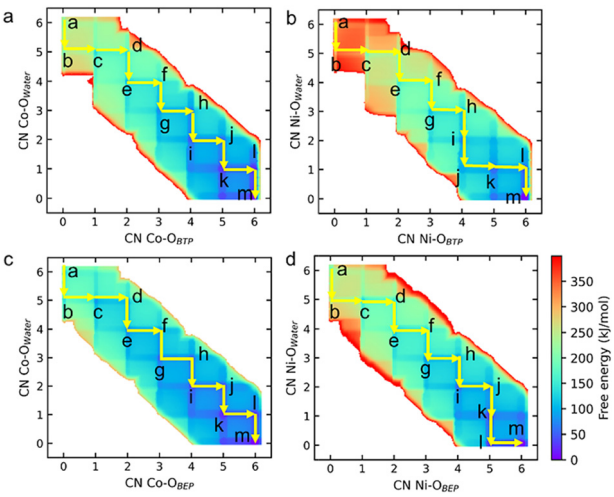

Fig. 6 Ligand substitution pathway mapped by the most thermodynamically favourable route at each step for systems of (a) BTP-Co^{2+}, (b) BTP-Ni^{2+}, (c) BEP-Co^{2+}, (d) BEP-Ni^{2+}. Labels a–m represent the corresponding intermediates and transition states along the pathway.

pathway patterns. The first substitution step proceeds *via* the vacate-and-fill route (CN = 6 → 5), whereas the subsequent steps mainly follow the oversaturate-and-release route (CN = 6 → 7). A possible reason is that, at the very early stage, the metal ion has a water-coordinated solvation shell and is located closer to the aqueous side, where the extractant ligands in the organic phase are less accessible. Losing the first coordinated water molecule is therefore easier than binding an extractant ligand. Once one or more extractant ligands have coordinated, the solvation cluster becomes more organophilic and shifts slightly toward the organic side, where extractant ligands are more accessible. In this environment, the insertion of additional extractant ligands becomes slightly easier than the dissociation of water. This behaviour is reflected in the unbiased z-coordinates of the metal ion. The ion is located closer to the aqueous side when the water coordination number is high and closer to the organic side when the coordination number of extractant ligands is high (Fig. S5).

First water-ligand substitution dictates selectivity

The first water–ligand substitution step governs the extraction in thermodynamics. We quantified the free-energy profiles along the optimal substitution pathways, as shown in Fig. 7a. All systems exhibit an overall decrease in free energy along the substitution pathway, with energy barriers appearing at certain steps. The maximum free-energy barrier occurs at the very first substitution step, *i.e.*, from (0,6) to (1,5). At this step, the vacate-and-fill route, where water first leaves to create a vacant site, dominates substitution (Fig. 6). These results suggest that removing the first water molecule from the solvation shell is the energy bottleneck of the entire substitution process.

The free energy variation associated with substituting the first water molecule determines the Co^{2+}/Ni^{2+} selectivity. We use the free-energy barrier to quantify the substitution steps during extraction because the barrier value represents the energy required for the substitution to occur. In both the BTP and BEP extraction systems, Co^{2+} exhibits lower free-energy barriers ΔF (19.0 kJ mol^{-1} for BTP, 33.0 kJ mol^{-1} for BEP) than Ni^{2+} (49.9 kJ mol^{-1} for BTP, 50.1 kJ mol^{-1} for BEP), as shown in Fig. 7b and Table 1. These results indicate that water–ligand substitution is energetically more favourable for Co^{2+} than for Ni^{2+}. As a result, Co^{2+} forms extractant-coordinated complexes more easily, which promotes its transfer into the organic phase over Ni^{2+}. Ni^{2+} is known to form shorter and more strongly bound aqua complexes than Co^{2+}.[31] The stronger hydration of Ni^{2+} is expected to impose a higher energy penalty for solvation shell disruption. The WT-MetaD results show that the first water-to-ligand substitution step has the highest barrier along the optimal pathway and the largest Co^{2+}/Ni^{2+} free-energy difference. Thus, the simulations identify the first solvation substitution step as the key energetic origin for ligand-dependent selectivity.

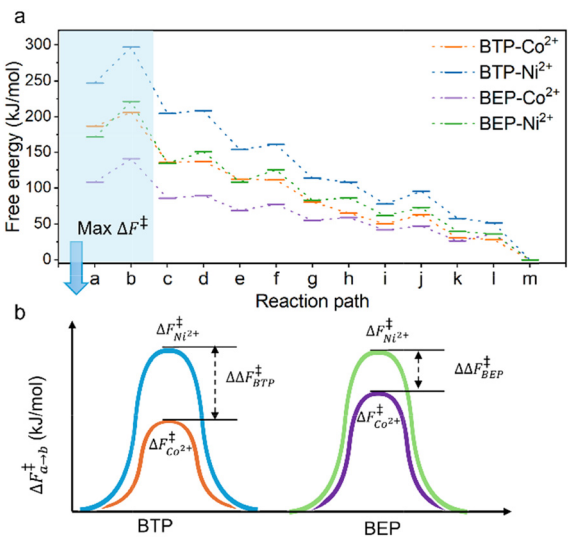

Fig. 7 (a) Free-energy profiles along the optimal ligand-substitution pathways. The maximum free-energy barriers (ΔF) are observed at the first ligand-substitution step. (b) Comparative metal-dependent free-energy barriers (ΔF) for Co^{2+} and Ni^{2+}, as well as the extractant-dependent relative free-energy differences ($\Delta\Delta F$) between BTP and BEP, are shown to illustrate the thermodynamic origin of selectivity.

Table 1 Free-energy barriers (ΔF) and ligand-induced relative free-energy differences ($\Delta\Delta F$) for the first substitution step, and the calculated Co^{2+}/Ni^{2+} selectivity, k

Extractant	Metal ion	ΔF (kJ mol^{-1})	$\Delta\Delta F$ (kJ mol^{-1})	Co^{2+}/Ni^{2+} selectivity, k
BTP	Co^{2+}	19.0	30.9	2.4×10^5
	Ni^{2+}	49.9		
BEP	Co^{2+}	33.0	17.1	9.5×10^2
	Ni^{2+}	50.1		

Extractant ligands tune the Co^{2+}/Ni^{2+} energy gap of the first-step substitution and thus confer selectivity. When comparing the two extractants, the relative free-energy differences ($\Delta\Delta F$) between Co^{2+} and Ni^{2+} can serve as an indicator of selectivity.[32,33] The selectivity k can be estimated using the expression:

$$k = e^{-\frac{\Delta F(Co^{2+}) - \Delta F(Ni^{2+})}{RT}},$$

where ΔF represents the maximum free-energy barrier of ligand substitution. The $\Delta\Delta F$ is higher for BTP (30.9 kJ mol^{-1}) than for BEP (17.1 kJ mol^{-1}), indicating that BTP imposes a stronger energetic discrimination between the two ions during first-step substitution. As a result, BTP is more effective in separating Co^{2+} from Ni^{2+} than BEP. This selectivity difference could be attributed to the electronic and structural features of the ligand's headgroups. The phosphinic moiety in BTP localizes greater negative charge density on the O^- donor, thereby strengthening coordination interactions with Co^{2+}.[8,34] Because Co^{2+} is more labile than Ni^{2+}, BTP's stronger O^- "hits Co^{2+} harder". Interfacial organization likely contributes as well. BTP's headgroup presents donor oxygens at the interface and exclude water more efficiently than BEP's phosphate-based assemblies, which tend to self-associate more strongly and are more prone to trapping water. This organization can reduce interfacial water accessibility and promote water elimination from the solvation shell.[10,35] These effects could amplify the free-energy gap between Co^{2+} and Ni^{2+}. Published extraction data show that extraction processes can selectively separate cobalt ions from nickel ions, and that BTP exhibits a

significantly higher Co^{2+}/Ni^{2+} separation factor than BEP.[36–40] For example, separation factors for BTP have been reported to be 10^2–10^3 times higher than those for BEP under optimized experimental conditions.[37] This level of difference is comparable to the selectivity estimated from our free-energy calculations, which indicate that BTP exhibits $\sim 2.5 \times 10^2$ times higher selectivity than BEP. Our results suggest that tailoring ligand chemistry to increase the $\Delta\Delta F$ associated with the first solvation-substitution step represents a viable target for solvent extraction design.

Conclusions

This work examined the thermodynamics of water–ligand substitution during the extraction of Co^{2+} and Ni^{2+} using the extractant ligands BTP and BEP. Spectroscopic measurements confirmed ligand substitution upon extraction, and MD simulations revealed six donor oxygen atoms in the first solvation shell of Co^{2+} and Ni^{2+} in both aqueous and organic solutions. We then calculated the free-energy landscapes of water–ligand substitution using WT-MetaD. The landscapes show that substitution proceeds stepwise and follows either a vacate-and-fill or an oversaturate-and-release route. In the vacate-and-fill route, a water molecule leaves the solvation shell to create a vacant coordination site, followed by ligand entry. In the oversaturate-and-release route, the ligand first coordinates to the metal ion and subsequently expels a water molecule. We mapped the full substitution pathways and quantified the free-energy changes. The first substitution step, during which the first water molecule in the solvation shell is substituted, exhibits the largest free-energy barrier ΔF. Disrupting the initial water solvation shell to bind the first extractant ligand is therefore the most energetically demanding event in the extraction process. The energy cost of this first substitution step dictates selectivity: Co^{2+} shows a lower ΔF than Ni^{2+}, explaining the selective extraction over Ni^{2+}. In addition, BTP exhibits a larger $\Delta\Delta F$ than BEP, indicating higher selectivity. This work demonstrates that substitution of the first water molecule controls extraction selectivity. Tuning ligand chemistry to maximize the relative energy gap at this step provides a plausible design target for optimizing metal solvent extraction.

Conflicts of interest

There are no conflicts to declare.

Data availability

The data supporting this article have been included as part of the supplementary information (SI). Supplementary information includes detailed methods, ion distributions in WT-MetaD simulations, stepwise free-energy barriers, and WT-MetaD convergence analyses. See DOI: https://doi.org/10.1039/d6cp00202a.

Input files for the MD and WT-MetaD simulations are available on Zenodo at https://doi.org/10.5281/zenodo.18146475.

Acknowledgements

This work was supported by the U.S. Department of Energy (DOE) under Award No. DE-SC0025346. This work used the Delta system at the National Center for Supercomputing Applications through allocation [CHM250076] from the Advanced Cyberinfrastructure Coordination Ecosystem: Services & Support (ACCESS) program, which is supported by National Science Foundation grants #2138259, #2138286, #2138307, #2137603, and #2138296. We thank the University of Kentucky Center for Computational Sciences and Information Technology Services Research Computing for their support and use of the Lipscomb Compute Cluster and associated research computing resources.

Notes and references

1 S. E. Can Sener, V. M. Thomas, D. E. Hogan, R. M. Maier, M. Carbajales-Dale, M. D. Barton, T. Karanfil, J. C. Crittenden and G. L. Amy, Recovery of critical metals from aqueous sources, *ACS Sustainable Chem. Eng.*, 2021, **9**, 11616–11634.
2 S. Krishnan, N. S. Zulkapli, H. Kamyab, S. M. Taib, M. F. B. M. Din, Z. Abd Majid, S. Chaiprapat, I. Kenzo, Y. Ichikawa and M. Nasrullah, Current technologies for recovery of metals from industrial wastes: An overview, *Environ. Technol. Innovation*, 2021, **22**, 101525.
3 G. Alvial-Hein, H. Mahandra and A. Ghahreman, Separation and recovery of cobalt and nickel from end of life products via solvent extraction technique: A review, *J. Cleaner Prod.*, 2021, **297**, 126592.
4 K. Kim, D. Raymond, R. Candeago and X. Su, Selective cobalt and nickel electrodeposition for lithium-ion battery recycling through integrated electrolyte and interface control, *Nat. Commun.*, 2021, **12**, 6554.
5 M. Špadina, J.-F. Dufrêche, S. Pellet-Rostaing, S. Marčelja and T. Zemb, Molecular forces in liquid–liquid extraction, *Langmuir*, 2021, **37**, 10637–10656.
6 L. S. Martins, S. Rovani and A. B. Botelho, Junior and D. C. Romano Espinosa, Sustainable approach for critical metals recovery through hydrometallurgical processing of spent batteries using organic acids, *Ind. Eng. Chem. Res.*, 2023, **62**, 18672–18682.
7 D. S. Flett, Solvent extraction in hydrometallurgy: the role of organophosphorus extractants, *J. Organomet. Chem.*, 2005, **690**, 2426–2438.
8 A. M. Wilson, P. J. Bailey, P. A. Tasker, J. R. Turkington, R. A. Grant and J. B. Love, Solvent extraction: the coordination chemistry behind extractive metallurgy, *Chem. Soc. Rev.*, 2014, **43**, 123–134.
9 A. Uysal, Aqueous interfaces in chemical separations, *Langmuir*, 2023, **39**, 17570–17580.
10 B. S. Dwadasi, S. G. Srinivasan and B. Rai, Interfacial structure in the liquid–liquid extraction of rare earth elements by phosphoric acid ligands: A molecular dynamics study, *Phys. Chem. Chem. Phys.*, 2020, **22**, 4177–4192.
11 Z. Liang, W. Bu, K. J. Schweighofer, D. J. Walwark Jr, J. S. Harvey, G. R. Hanlon, D. Amoanu, C. Erol, I. Benjamin and

M. L. Schlossman, Nanoscale view of assisted ion transport across the liquid–liquid interface, *Proc. Natl. Acad. Sci. U. S. A.*, 2019, **116**, 18227–18232.

12 E. Scoppola, E. B. Watkins, R. A. Campbell, O. Konovalov, L. Girard, J. F. Dufrêche, G. Ferru, G. Fragneto and O. Diat, Solvent extraction: Structure of the liquid–liquid interface containing a diamide ligand, *Angew. Chem.*, 2016, **128**, 9472–9476.

13 Z. Liang, T. Vo, K. J. Schweighofer, I. Benjamin and M. L. Schlossman, DEHP− extractant binding to trivalent lanthanide Er^{3+}: Fast binding accompanied by concerted angular motions of hydration water, *J. Chem. Phys.*, 2023, **158**, 134715.

14 H. Watarai and H. Freiser, Role of the interface in the extraction kinetics of zinc and nickel ions with alkyl-substituted dithizones, *J. Am. Chem. Soc.*, 1983, **105**, 189–190.

15 W. Bu, H. Yu, G. Luo, M. K. Bera, B. Hou, A. W. Schuman, B. Lin, M. Meron, I. Kuzmenko and M. R. Antonio, Observation of a rare earth ion–extractant complex arrested at the oil–water interface during solvent extraction, *J. Phys. Chem. B*, 2014, **118**, 10662–10674.

16 Q.-W. Meng, X. Zhu, W. Xian, S. Wang, Z. Zhang, L. Zheng, Z. Dai, H. Yin, S. Ma and Q. Sun, Enhancing ion selectivity by tuning solvation abilities of covalent-organic-framework membranes, *Proc. Natl. Acad. Sci. U. S. A.*, 2024, **121**, e2316716121.

17 R. Kingsbury, A guide to ion separations for the global energy transition, *Joule*, 2025, **9**, 102134.

18 L. Helm and A. Merbach, Water exchange on metal ions: experiments and simulations, *Coord. Chem. Rev.*, 1999, **187**, 151–181.

19 A. Barducci, M. Bonomi and M. Parrinello, Metadynamics, *Wiley Interdiscip. Rev.: Comput. Mol. Sci.*, 2011, **1**, 826–843.

20 A. Barducci, G. Bussi and M. Parrinello, Well-tempered metadynamics: a smoothly converging and tunable free-energy method, *Phys. Rev. Lett.*, 2008, **100**, 020603.

21 X. Wang, A. A. Peroutka, D. V. Kravchuk, J. C. Shafer, R. E. Wilson and M. J. Servis, Metadynamics investigation of lanthanide solvation free energy landscapes and insights into separations energetics, *Chem. Sci.*, 2024, **15**, 16494–16502.

22 E. Méndez and R. Semino, Thermodynamic insights into the self-assembly of zeolitic imidazolate frameworks from computer simulations, *Chem. Sci.*, 2025, **16**, 11979–11988.

23 I. Van De Voorde, L. Pinoy, E. Courtijn and F. Verpoort, Influence of acetate ions and the role of the diluents on the extraction of copper(II), nickel(II), cobalt(II), magnesium(II) and iron (II, III) with different types of extractants, *Hydrometallurgy*, 2005, **78**, 92–106.

24 A. J. M. Santanilla, P. Aliprandini, J. Benvenuti, J. A. S. Tenorio and D. C. R. Espinosa, Structure investigation for nickel and cobalt complexes formed during solvent extraction with the extractants Cyanex 272, Versatic 10 and their mixtures, *Miner. Eng.*, 2021, **160**, 106691.

25 K. Staszak, M. Regel-Rosocka, K. Wieszczycka and P. Burmistrzak, Copper(II) sulphate solutions treatment by solvent extraction with Na-Cyanex 272, *Sep. Purif. Technol.*, 2012, **85**, 183–192.

26 D. H. Fatmehsari, D. Darvishi, S. Etemadi, A. E. Hollagh, E. K. Alamdari and A. Salardini, Interaction between TBP and D2EHPA during Zn, Cd, Mn, Cu, Co and Ni solvent extraction: A thermodynamic and empirical approach, *Hydrometallurgy*, 2009, **98**, 143–147.

27 D. Z. Caralampio, B. Reeves, M. R. Beccia, J. M. Martínez, R. R. Pappalardo, C. den Auwer and E. Sánchez Marcos, Revisiting the cobalt(II) hydration from molecular dynamics and X-ray absorption spectroscopy, *Mol. Phys.*, 2019, **117**, 3320–3328.

28 H. Liu, C. Fang, Y. Fang, Y. Zhou, H. Ge, F. Zhu, P. Sun and J. Miao, Characterizing Ni(II) hydration in aqueous solution using DFT and EXAFS, *J. Mol. Model.*, 2016, **22**, 2.

29 M. Busato, A. Lapi, P. D'Angelo and A. Melchior, Coordination of the Co2+ and Ni2+ Ions in Tf2N–Based Ionic Liquids: A Combined X-ray Absorption and Molecular Dynamics Study, *J. Phys. Chem. B*, 2021, **125**, 6639–6648.

30 R. D. Shannon, Revised effective ionic radii and systematic studies of interatomic distances in halides and chalcogenides, *Found. Crystallogr.*, 1976, **32**, 751–767.

31 P. D'Angelo, V. Barone, G. Chillemi, N. Sanna, W. Meyer-Klaucke and N. V. Pavel, Hydrogen and higher shell contributions in Zn^{2+}, Ni^{2+}, and Co^{2+} aqueous solutions: An X-ray absorption fine structure and molecular dynamics study, *J. Am. Chem. Soc.*, 2002, **124**, 1958–1967.

32 O. Gutten and L. Rulisek, Predicting the stability constants of metal-ion complexes from first principles, *Inorg. Chem.*, 2013, **52**, 10347–10355.

33 P. Chatterjee, W. M. Botello-Smith, H. Zhang, L. Qian, A. Alsamarah, D. Kent, J. J. Lacroix, M. Baudry and Y. Luo, Can relative binding free energy predict selectivity of reversible covalent inhibitors?, *J. Am. Chem. Soc.*, 2017, **139**, 17945–17952.

34 Z. Li, B. Onghena, X. Li, Z. Zhang and K. Binnemans, Enhancing metal separations using hydrophilic ionic liquids and analogues as complexing agents in the more polar phase of liquid–liquid extraction systems, *Ind. Eng. Chem. Res.*, 2019, **58**, 15628–15636.

35 K. Omelchuk, M. Stambouli and A. Chagnes, Investigation of aggregation and acid dissociation of new cationic exchangers for liquid-liquid extraction, *J. Mol. Liq.*, 2018, **262**, 111–118.

36 B. R. Reddy and K. H. Park, Process for the recovery of cobalt and nickel from sulphate leach liquors with saponified Cyanex 272 and D2EHPA, *Sep. Sci. Technol.*, 2007, **42**, 2067–2080.

37 N. Devi, K. Nathsarma and V. Chakravortty, Separation and recovery of cobalt(II) and nickel(II) from sulphate solutions using sodium salts of D2EHPA, PC 88A and Cyanex 272, *Hydrometallurgy*, 1998, **49**, 47–61.

38 K. Sarangi, B. Reddy and R. Das, Extraction studies of cobalt(II) and nickel(II) from chloride solutions using Na-Cyanex 272.: Separation of Co(II)/Ni(II) by the sodium salts of D2EHPA, PC88A and Cyanex 272 and their mixtures, *Hydrometallurgy*, 1999, **52**, 253–265.

39 Y. Liu, S. H. Nam and M. S. Lee, A Study on the separation of Co(II), Ni(II), and Mg(II) by solvent extraction with cationic extractants, *Bull. Korean Chem. Soc.*, 2015, **36**, 2646–2650.

40 J. Wang, J. Fu, F. Yu, W. Xu and H. Wang, An efficient extractant (2-ethylhexyl)(2, 4, 4′-trimethylpentyl) phosphinic acid (USTB-1) for cobalt and nickel separation from sulfate solutions, *Sep. Purif. Technol.*, 2020, **248**, 117060.